Click Here for Full Article

Effects of lateral viscosity variations on the geoid

A. Ghosh,[1] T. W. Becker,[1] and S. J. Zhong[2]

[1]   We investigate the effects of lateral viscosity variations (LVVs) on mantle circulation model predictions of the global geoid. The present study is motivated in part by earlier findings that LVVs due to stiff slabs in the lower mantle have a strong influence on the geoid, and that slabs in the lower mantle are perhaps no stronger than the ambient mantle. However, more recently, it has been argued based on global seismic tomography models that LVVs are a minor effect on the geoid. In the light of these seemingly contradictory results, we re-visit the problem of slab strength in the lower mantle. We substantiate that the geoid calculated from tomography is hardly affected by the presence of LVVs, whereas the geoid computed from global slab models yields a poor fit to the observed geoid when LVVs are considered. However, this degradation of fit only occurs for very long wavelengths of flow, indicating inherent differences between the slab and tomography models. We also investigate the effects on the geoid due to weak plate boundaries, strong cratonic keels, and a low viscosity region in the D'' layer due to post-perovskite. In addition to the geoid, we attempt to fit plate motions with a circulation model that has prescribed weak zones at plate boundaries. Motions are matched well and, taking into account LVVs, the geoid with appropriate surface velocity boundary conditions agrees with the observed geoid as well as for free slip cases. Citation: Ghosh, A., T. W. Becker, and S. J. Zhong (2010), Effects of lateral viscosity variations on the geoid, Geophys. Res. Lett., 37, L01301, doi:10.1029/2009GL040426.

1.   Introduction

[2]   The long-wavelength geoid provides information regarding the density and viscosity within the Earth's mantle. The sensitivity of the geoid on the radial viscosity variations (RVVs) of the Earth is well documented [e.g., Richards and Hager, 1984], and the most prominent result is perhaps a viscosity increase in the lower mantle (LM). However, the effect of LVVs on the geoid is a subject of debate. Early 2-D work argued for a small effect of LVVs [e.g., King and Hager, 1994], but LVVs were found to be important for 3-D flow [Zhang and Christensen, 1993; Cadek and Fleitout, 2003]. The present study is mainly motivated by Zhong and Davies [1999], who found that introducing even moderately stiff slabs in the LM degrades the geoid fit compared to a model with only RVVs. This would indicate that slabs in the LM are no stronger than the ambient mantle, which is somewhat contrary to expectations. On the other hand, Moucha et al. [2007] argued that LVVs inferred from seismic tomography have a minor effect on the geoid. In this study, we re-investigate the problem of the geoid response to LVVs and provide a comprehensive and quantitative assessment.

[3]   Besides slab strength, the geoid is also likely to be affected by other sources of LVVs arising e.g. from weak plate boundaries and strong lithospheric keels. Recently, Tosi et al. [2009a, 2009b] have argued that low viscosity post-perovskite (Ppv) within slabs at the CMB can potentially have a large effect on the geoid. We investigate the sensitivity of the geoid for each of these LVV sources separately. We also evaluate plate motions, which are influenced by LVVs. It has been suggested by Thoraval and Richards [1997] that free slip models yield a significantly better fit to the geoid compared to prescribed plate motion models. However, this is potentially due to lack of appropriate LVVs. We, therefore, examine the geoid in presence of LVVs with both imposed and dynamically generated velocity boundary conditions and compare the fit.

2.   Method

[4]   We used the finite element code CitcomS [Zhong et al., 2000], with an average horizontal resolution of 0.6 × 0.6 degree, to obtain the geoid up to spherical harmonic degree 31, including the effects of self-gravitation. Results were benchmarked against a Hager and O'Connell [1981] (HC) type solution method for RVVs. We used four density models: the slab models LRR98D [Ricard et al., 1993; Lithgow-Bertelloni and Richards, 1998] and STB00D [Steinberger, 2000], the composite tomography model SMEAN [Becker and Boschi, 2002] with the high density anomalies in the top 300 km below the cratons removed, and the TX2008 S-wave tomography model of Simmons et al. [2007]. A fifth model, the regionalized upper mantle (RUM) slab model of Gudmundsson and Sambridge [1998] was used in conjunction with the SMEAN tomography model in the LM. A velocity-density scaling ($dln\rho/dlnv_s$) of 0.25 was used for the tomography models throughout the mantle.

[5]   For most models, we used a four layer radial viscosity structure divided into lithosphere (0–100 km), upper mantle (UM) (100–410 km), transition zone (TZ) (410–660 km) and LM (660 km-CMB). For each density model, we optimized the radial viscosity that provided the best fit to the observed geoid by conducting a parameter space search using the HC method. Since the objective of the paper is to understand the effect of LVVs, and not necessarily to construct a "real Earth" model, besides the viscosity structure no other parameters were adjusted. Relative variations should thus be more meaningful than absolute fits, assuming that inversions are not biased by being stuck in a

---

[1]Department of Earth Sciences, University of Southern California, Los Angeles, California, USA.
[2]Department of Physics, University of Colorado, Boulder, Colorado, USA.
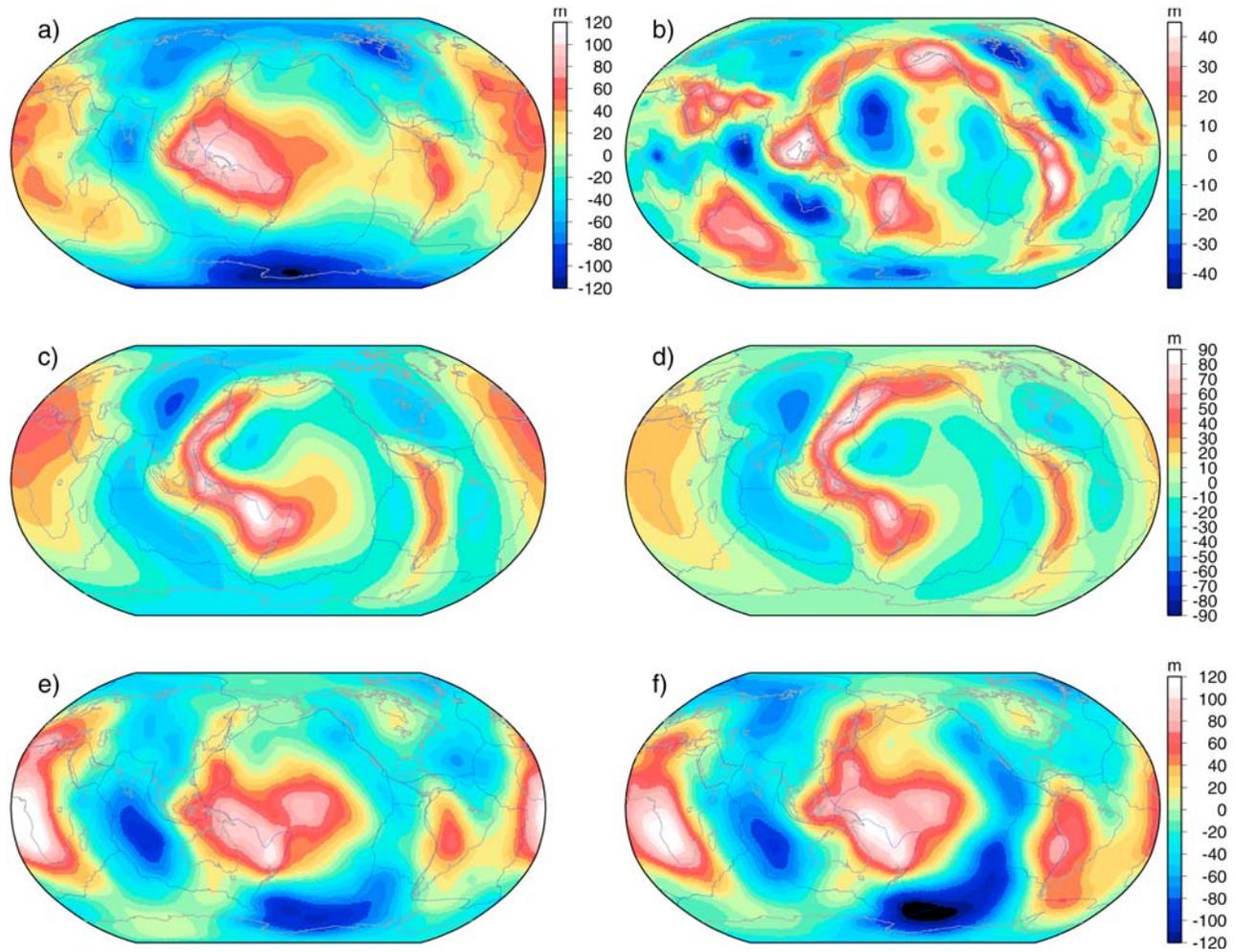
Figure 1. Observed geoid for (a) $l = 2-31$ and (b) $l = 4-12$. Computed geoid for $l = 2-31$ from LRR98D slab model with (c) radial and (d) lateral viscosity distribution and SMEAN tomography model with (e) radial and (f) lateral viscosity variations.

local minimum, against which we tested with parameter space exploration for various combinations of RVVs and LVVs. Some radial viscosity structures that yielded a poor fit to the geoid improved in fit when lateral variations in the top 100 km were considered. We also tested a few cases ("TBL cases") where we introduced a low viscosity (10 and 100 times weaker than the LM) layer between 2600 km and the CMB to take into account the effect of the lower thermal boundary layer [e.g., *Steinberger and Calderwood*, 2006].

[6] LVVs were introduced in two ways. First, viscosities were allowed to vary with temperature, as $\eta = \eta_0 \cdot \exp(E(T_0 - T))$. Here, T_0 and T are the reference and non-dimensionalized temperatures and E determines how strong the temperature dependence is; we took care to maintain the same average layer viscosity for the temperature-dependent as well as the radial cases. To introduce the effect of Ppv, a reverse temperature dependence was assigned to depths between 2600 km and CMB. The geoid was computed and correlated for each spherical harmonic degree with the observed geoid (Figure 1a) [*Mayer-Guerr*, 2006], corrected for the hydrostatic shape following *Nakiboglu* [1982]. A regional geoid was also computed over subduction zones by filtering the geoid through a subduction zone filter based on the slab models.

[7] In the second method, specific viscosity values were assigned to certain tectonic regions. Viscosities 100 times lower than the intraplate regions were assigned to the plate margins down to 100 km to examine the influence of weak plate boundaries. The effect of stiff cratons was tested by assigning 100 times higher than ambient viscosities to 3SMAC cratons [*Nataf and Ricard*, 1996] down to 300 km, with the density anomalies beneath the cratons removed. All models were calculated with free slip boundary conditions, except in one case, when plate velocities from NUVEL-1A [*DeMets et al.*, 1990] in the NNR frame were imposed as surface boundary condition for comparison. We tracked the change of geoid magnitudes with introduction of LVVs by calculating the ratios of the LVV and radial geoid RMS. A "regional RMS" was also computed in order to study the change in geoid magnitude over subduction zones using the aforementioned regionalization.

3. Strength of Slabs in the Lower Mantle

[8] We first evaluated the geoid for the LRR98D slab and the SMEAN density models with RVVs only ("LRR98D_radial" and "SMEAN_radial"). As expected, geoid highs were found over most of the subduction zones and both
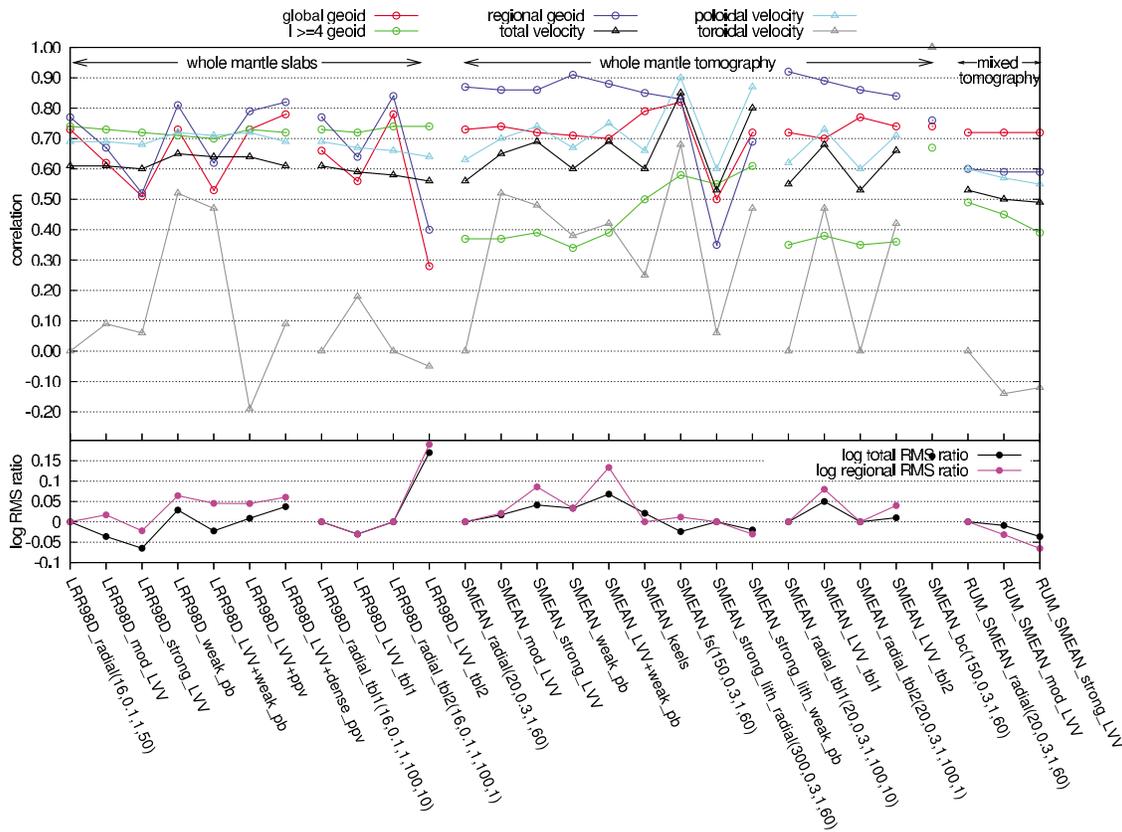
Figure 2. (top) Plot of the correlation coefficient between observations and predictions for all the model combinations. (bottom) Log of RMS ratios between geoid from RVV and LVV distribution. The geoid symbols are open circles, whereas open triangles are used for velocities. The points from models with the same density structure are connected with lines. Note that for the model with imposed plate motions (SMEAN_bc) the velocity correlations are unity. The "regional geoid" calculated is the geoid over subduction zones. The radial distribution for the models are given within brackets. The models, for which the radial viscosity distribution are not shown, have the same viscosity structure as the one immediately preceding them. The cases with modelname followed by "tbl (1 or 2)" have a low viscosity layer close to the CMB.

yielded comparable fit (0.73 and 0.725, Figures 1c and 1e) to the observed geoid (Figure 1a). Correlations could be improved, e.g. by assuming depth-dependent density scaling, however, we are not concerned with such optimization. Next, we introduced moderate LVVs (slabs/high density anomalies ∼ 150 times stiffer than ambient). In this case, while the correlation to the geoid increased slightly for SMEAN (0.74, "SMEAN_mod_LVV"), the correlation degraded substantially for slabs (0.62, "LRR98D_mod_LVV", "global geoid" line in Figure 2). On introduction of stronger LVVs (slabs/high density anomalies ∼1000 times stiffer than ambient, "LRR98D_strong_LVV" and "SMEAN_strong_LVV"), the fit for slabs degraded further (0.51, Figures 1d and 2), whereas the fit remained almost the same for SMEAN (0.72, Figures 1f and 2). For the LRR98D case, the geoid highs over subduction zones became more pronounced in the North Pacific, contrary to observations. The correlation over subduction zones ("regional geoid") degraded (Figure 2) and the geoid high over Africa also decreased. The above results are consistent with the findings of Zhong and Davies [1999], who showed that the geoid highs over subduction zones can be produced by stiff isolated slabs that enhance the flow coupling to the CMB, giving rise to less pronounced topographic lows over subduction zones, producing more positive geoid. For the

SMEAN model, the amplitude of the geoid over subduction zones increased with LVVs. However, the overall pattern was only slightly different between the RVV and LVV cases, which is in agreement with the observation of Kaban et al. [2007] and Moucha et al. [2007]. Performing the same set of tests on models STB00D and TX2008 showed similar trends. For the "TBL cases", the results were consistent with the findings of the non-TBL models (Figure 2).

[9] Additionally, we tested a combined model with seismicity-based RUM slabs in the UM and SMEAN tomography in the LM (RUM_SMEAN) [Yoshida and Nakakuki, 2009]. The global correlation to the observed geoid changed very slightly as in the pure SMEAN cases. Calculation of regional correlation over subduction zones showed an almost constant fit for "RUM_SMEAN" for both RVV and LVV cases and an overall decrease in the geoid magnitudes over subduction zones when LVVs were introduced (Figure 2).

[10] Since the wavelengths that are most sensitive to the presence of slabs are between degrees 4–12 [Hager, 1984], we also filtered out $l = 2-3$ and $l > 12$ from the total geoid. On removing those wavelengths, the subduction zone signal became more pronounced (Figure 1b), although the overall geoid amplitudes dropped. We then filtered the longest and shorter wavelengths from the computed geoid for both

LRR98D and SMEAN for RVV and LVV cases. The resultant $l = 4-12$ geoid from LRR98D showed similar fit to the observed geoid for $l = 4-12$ (Figure 1b), for both the RVV (0.73) and LVV cases (0.73 and 0.72 for moderate and strong temperature dependent viscosity, "$l \geq 4$ geoid" line in Figure 2). For SMEAN, the overall fit decreased when the longest wavelengths were subtracted, however, the relative fits between the RVV and LVV cases remained almost unchanged. Similar trends were seen with models STB00D and TX2008. It could be argued that the lowest degrees contain significant power for the slab and tomography models, hence, filtering them out would also remove a large part of the slab signal. Thus, we also compared the geoid from slab and tomography models with the observed geoid for $l = 2-3$, which would have most of its slab signal removed. The $l = 2-3$ geoid from both the models correlated well with the observed geoid for the radial cases (0.81), and so did the LVV geoid for the SMEAN model (0.83). However, the LVV geoid from LRR98D fared poorly (0.59) at those degrees, demonstrating that there exist inherent differences between the slab and tomography models, especially at low degrees, which are enhanced with the introduction of LVVs. The above differences between the models stem mainly from the presence of low density anomalies in the tomography models, and associated upwellings, especially in the Pacific region, which are absent in the slab models, and also from the different distribution of high density anomalies (slabs) in the two models.

[11] The global ($l = 2-31$) geoid from the slab model (Figures 1c and 1d) resembles the $l = 4-12$ observed geoid (Figure 1b), whereas, the global geoid from tomography (Figures 1e and 1f) resembles the global observed geoid (Figure 1a). Further inspection also reveals that the ring of positive geoid surrounding the Pacific in Figure 1b is better represented by the slab model with LVVs (Figure 1d) compared to the one with RVVs (Figure 1c). This indicates that the effect of strong slabs on the geoid depends on the wavelengths that are considered. When compared to the global observed geoid, the LVVs in the slab models degrade the fit, whereas if the longest wavelengths are removed from the observed geoid, in order to concentrate on the wavelengths that the slabs are sensitive to, the stiff LM slabs seem to match the geoid pattern better, although a quantitative assessment could not be done for this particular case. Hence, studies with regional models of slabs [see *Moresi and Gurnis*, 1996] would be required to draw any conclusion regarding slab strength.

4. Effects of Weak Plate Boundaries, Strong Continental Keels and Low Viscosity Post-Perovskite

[12] *Tosi et al.* [2009a, 2009b] pointed out that the presence of low viscosity Ppv beneath the slabs [*Hunt et al.*, 2009] could have a large effect on the geoid by reducing the geoid highs over subduction zones. This would allow for stiff slabs in the LM without having unrealistically high geoid over areas of subduction. We introduced such low viscosity Ppv beneath the slabs between 2600 km and CMB. The Ppv was made 1000 times weaker than the TZ by assigning a negative temperature dependent viscosity, with a normal temperature dependent viscosity in the

remaining four layers as before (LRR98D_strong_LVV). We found that global correlation returned to the radial case value (0.73); in spite of the presence of strong slabs, the fit to the global geoid did not degrade, as suggested by *Tosi et al.* [2009a, 2009b]. The same exercise repeated with a slightly denser Ppv (following *Tosi et al.* [2009b], "LRR98D_LVV+dense_ppv") produced similar results (Figure 2). The longest wavelengths ($l = 2, 3$) that yielded a degraded fit to the observed geoid when LVVs due to slabs were introduced, were influenced by the presence of the weak Ppv, which counteracted the effects of the strong slabs providing a good match with the observed geoid.

[13] Several earlier studies have discussed the importance of weak plate boundaries in influencing the geoid [e.g., *Zhong and Davies*, 1999; *Yoshida and Nakakuki*, 2009; *Tosi et al.*, 2009a, 2009b]. We introduced weak plate boundaries in our SMEAN tomography model. The geoid pattern due to LVVs from weak plate boundaries was not much affected: the global correlation decreased slightly, although the geoid magnitude changed considerably, especially, over the subduction zones where the geoid highs became more pronounced. We next tested a stronger lithospheric viscosity (300 times stronger than the TZ). The radial case (SMEAN_strong_lith_radial) showed a low correlation (0.50 in Figure 2) which improved considerably (0.71) with the inclusion of weak plate boundaries (SMEAN_strong_lith_weak_pb); the geoid highs over some subduction zones, which were absent in the radial case, could be reproduced by including weak plate margins, as shown previously by *Zhong and Davies* [1999].

[14] The effect of stiff continental keels on the geoid has been studied, e.g., by *Karpychev and Fleitout* [2000], who concluded that stiff keels have considerable impact on the long wavelength geoid, and also by *Zhong* [2001], who found the keels to be more important for regional scale geoid. We studied the effect of stiff continental keels on the geoid by incorporating high viscosity cratons in our SMEAN tomographic model (SMEAN_keels). An improved match with the observed geoid was seen when these stiff keels were considered. The correlation rose from 0.73 to 0.79. The main change occurred over North America, where inclusion of the keels resulted in a low geoid [see *Zhong*, 2001], as is observed, compared to the geoid high seen in that area from the radial case. The overall geoid magnitude increased slightly from the radial case whereas the geoid magnitude over subduction zones remained unchanged (Figure 2).

5. Predicting Plate Motions

[15] A comprehensive mantle circulation model should not only match the geoid, but also predict other indicators of convective flow, such as plate motions. LVVs are crucial in predicting the right plate motions [e.g., *Ricard and Vigny*, 1989; *Zhong et al.*, 2000]. We found that a strong lithosphere (150 times stronger than TZ) with weak plate boundaries, high viscosity cratonic keels and strong temperature dependent viscosities (SMEAN_fs) provided a good fit to both the observed geoid (0.82) and plate velocities (0.85, Figure 2), consistent with the findings of *Becker* [2006]. Hence, presence of LVVs permits a strong lithosphere, which otherwise produces a poor geoid fit, and

which is necessary in order to generate the right plate motions.

[16] We therefore expect that when an appropriate LVV and density structure is taken into consideration in the circulation model, the geoid with imposed plate velocities at the surface would yield a fit similar to the free slip case, unlike what has been suggested before [*Thoraval and Richards*, 1997]. In order to test this, we considered the viscosity structure that matched both plate velocities and geoid (SMEAN_fs) and calculated the geoid from this particular case, but this time after imposing plate velocities as surface boundary condition (SMEAN_bc). The resultant geoid showed a global correlation of 0.74 with the observed geoid, indicating that a good match is indeed possible with imposed velocity boundary conditions. It is our conjecture that tuning of parameters could improve the geoid fit further and that in the presence of LVVs, no additional requirements, such as a barrier to flow at 660 km [*Cadek and Fleitout*, 2003], are required to match dynamic observables within the context of whole mantle circulation.

[17] We also looked at how the presence of LVVs affect dynamic topography. The dynamic topography pattern did not vary much between RVV and LVV cases, however, the magnitudes were affected by as much as ∼20% when LVVs were introduced.

6. Conclusions

[18] High viscosity slabs in the LM have a large influence on the global geoid fit for slab-only models, whereas tomography models are insensitive to strong LVVs in the LM, confirming earlier work. However, when the geoid from slab and tomography models was compared with the observed geoid between degrees 4–12, in order to focus on the slab response, it was found that the fit remained unchanged between cases of radial and lateral viscosity variations for both slab and tomography models. This reconciles the findings of *Zhong and Davies* [1999] and *Moucha et al.* [2007]. A comparison of the low degree geoid ($l = 2–3$) showed a substantial change in geoid pattern with LVVs for slab-only models, indicating that differences in the slab and tomography models, especially the absence of low velocity anomalies in the former, are enhanced by the introduction of LVVs. This implies that the slab model may not be an adequate description of the overall mantle buoyancy forces.

[19] Weak plate boundaries affect both the style and amplitude of the geoid as long as the lithosphere is sufficiently stiff and are hence important for global plate dynamics. Presence of stiff continental keels improves the geoid fit. A model with weak plate boundaries in addition to temperature dependent viscosity and strong cratonic keels provided a good match to both the observed geoid and plate motions; imposing surface velocity boundary conditions instead to the same model yielded similar results. A strong lithosphere, which is important to match plate motions, and which otherwise provides a poor fit to the geoid, is possible when LVVs are considered. This implies that circulation models with LVVs that assume simple whole mantle flow are consistent with geoid and velocity constraints.

References

Becker, T. W. (2006), On the effect of temperature and strain-rate viscosity on global mantle flow, net rotation, and driving forces, *Geophys. J. Int.*, *167*, 943–957.

Becker, T. W., and L. Boschi (2002), A comparison of tomographic and geodynamic mantle models, *Geochem. Geophys. Geosyst.*, *3*(1), 1003, doi:10.1029/2001GC000168.

Cadek, O., and L. Fleitout (2003), Effect of lateral viscosity variations in the top 300 km on the geoid and dynamic topography, *Geophys. J. Int.*, *152*, 566–580.

DeMets, C., R. G. Gordon, D. F. Argus, and S. Stein (1990), Current plate motions, *Geophys. J. Int.*, *101*, 425–478.

Gudmundsson, O., and M. Sambridge (1998), A regionalized upper mantle (RUM) seismic model, *J. Geophys. Res.*, *103*, 7121–7136.

Hager, B. H. (1984), Subducted slabs and the geoid: Constraints on mantle rheology and flow, *J. Geophys. Res.*, *89*, 6003–6015.

Hager, B. H., and R. J. O'Connell (1981), A simple global model of plate dynamics and mantle convection, *J. Geophys. Res.*, *86*, 4843–4878.

Hunt, S. A., D. J. Weidner, L. Li, L. Wang, N. P. Walte, J. P. Brodholt, and D. P. Dobson (2009), Weakening of calcium iridate during its transformation from perovskite to post-perovskite, *Nature Geosci.*, *2*, doi:10.1038/ngeo663.

Kaban, M., I. Rogozhina, and V. Trubitsyn (2007), Importance of lateral viscosity variations in the whole mantle for modelling of the dynamic geoid and surface velocities, *J. Geodyn.*, *43*, 262–273.

Karpychev, M., and L. Fleitout (2000), Long-wavelength geoid: The effect of continental roots and lithosphere thickness variations, *Geophys. J. Int.*, *143*, 945–963.

King, S. D., and B. H. Hager (1994), Subducted slabs and the geoid: 1. Numerical experiments with temperature-dependent viscosity, *J. Geophys. Res.*, *99*, 19,843–19,852.

Lithgow-Bertelloni, C., and M. Richards (1998), The dynamics of Cenozoic and Mesozoic plate motions, *Rev. Geophys.*, *36*, 27–78.

Mayer-Guerr, T. (2006), Gravitationsfeldbestimmung aus der analyse kurzer Bahnbögen am Beispiel der Satellitenmissionen CHAMP und GRACE, Ph.D. thesis, Univ. of Bonn, Bonn, Germany.

Moresi, L. N., and M. Gurnis (1996), Constraints on the lateral strength of slabs from three-dimensional dynamic flow models, *Earth Planet. Sci. Lett.*, *138*, 15–28.

Moucha, R., A. Forte, J. Mitrovica, and A. D. Daradich (2007), Lateral variations in mantle rheology: Implications for convection related surface observables and inferred viscosity models, *Geophys. J. Int.*, *169*, 113–135.

Nakiboglu, S. M. (1982), Hydrostatic theory of the Earth and its mechanical implications, *Phys. Earth Planet. Int.*, *28*, 302–311.

Nataf, H., and Y. Ricard (1996), 3SMAC: An a priori tomographic model of the upper mantle based on geophysical modeling, *Phys. Earth Planet. Inter.*, *95*, 101–122.

Ricard, Y., and C. Vigny (1989), Mantle dynamics with induced plate tectonics, *J. Geophys. Res.*, *94*, 5987–6002.

Ricard, Y., M. Richards, C. Lithgow-Bertelloni, and Y. Le (1993), A geodynamic model of mantle density heterogeneity, *J. Geophys. Res.*, *98*, 21,895–21,909.

Richards, M. A., and B. H. Hager (1984), Geoid anomalies in a dynamic Earth, *J. Geophys. Res.*, *89*, 10,299–10,313.

Simmons, N. A., A. M. Forte, and S. P. Grand (2007), Thermochemical structure and dynamics of the African superplume, *Geophys. Res. Lett.*, *34*, L02301, doi:10.1029/2006GL028009.

Steinberger, B. (2000), Slabs in the lower mantle: Results of dynamic modelling compared with tomographic images and the geoid, *Phys. Earth Planet. Inter.*, *2000*, 241–257.

Steinberger, B., and A. Calderwood (2006), Models of large-scale viscous flow in the Earth's mantle with constraints from mineral physics and surface observations, *Geophys. J. Int.*, *167*, 1461–1481, doi:10.1111/j.1365-246X.2006.03131.x.

Thoraval, C., and M. A. Richards (1997), The geoid constraint in global geodynamics: Viscosity structure, mantle heterogeneity models, and boundary conditions, *Geophys. J. Int.*, *131*, 1–8.

Tosi, N., O. Cadek, and Z. Martinec (2009a), Subducted slabs and lateral viscosity variations: Effects on the long wavelength geoid, *Geophys. J. Int.*, *179*, 813–826, doi:10.1111/j.1365-246X.2009.04335.x.

Tosi, N., O. Cadek, Z. Martinec, D. A. Yuen, and G. Kaufmann (2009b), Is the long-wavelength geoid sensitive to the presence of postperovskite above the core-mantle boundary?, *Geophys. Res. Lett.*, *36*, L05303, doi:10.1029/2008GL036902.

Yoshida, M., and T. Nakakuki (2009), Effects on the long-wavelength geoid anomaly of lateral viscosity variations caused by stiff subducting slabs, weak plate margins and lower mantle rheology, *Phys. Earth Planet. Inter.*, *172*, 278–288.

Zhang, S., and U. Christensen (1993), Some effects of lateral viscosity variations on geoid and surface velocities induced by density anomalies in the mantle, *Geophys. J. Int.*, *114*, 531–547.

Zhong, S. (2001), Role of ocean-continent contrast and continental keels on plate motion, net rotation of lithosphere, and the geoid, *J. Geophys. Res.*, *106*, 703–712.

Zhong, S., and G. Davies (1999), Effects of plate and slab viscosities on the geoid, *Earth Planet. Sci. Lett.*, *170*, 487–496.

Zhong, S., M. T. Zuber, L. N. Moresi, and M. Gurnis (2000), The role of temperature-dependent viscosity and surface plates in spherical shell models of mantle convection, *J. Geophys. Res.*, *105*, 11,063–11,082.

_____

T. W. Becker and A. Ghosh, Department of Earth Sciences, University of Southern California, 3651 Trousdale Pkwy., Los Angeles, CA 90089-0740, USA. (attreyeg@usc.edu)

S. J. Zhong, Department of Physics, University of Colorado, Boulder, CO 80309-0390, USA.